Development of Mg-Based Superelastic Alloy Through Aging Heat Treatment

Keisuke Yamagishi, Yukiko Ogawa, Daisuke Ando, and Yuji Sutou

Abstract

The effect of aging heat treatment on microstructure, hardness, and superelasticity at room temperature was investigated herein for Mg-18.8 at.% Sc alloy. The hardness of the alloy is increased via aging heat treatment at temperatures between 423 and 523 K, from ∼ 90 Hv (as-quenched condition) to a maximum of 180 Hv. Aging heat treatment at a higher temperature reduces the incubation time before the onset of age hardening. Scanning electron microscopy observations and X-ray diffraction analysis showed that the precipitation of hexagonal close-packed (α) phases within the body-centered cubic (β) matrix phase causes age hardening and the hardness value almost depends linearly on the volume fraction of α precipitates. Furthermore, the α precipitates formed via aging heat treatment can be deformed along with β matrix phase upon stress-induced martensitic transformation in a sample with ∼ 10% volume fraction of α precipitates, resulting in a slight reduction in stress hysteresis and a minor increase in superelastic recovery compared with the as-quenched condition.

K. Yamagishi · D. Ando (✉) · Y. Sutou
Department of Materials Science, Graduate School of Engineering, Tohoku University, 6-6-11 Aoba, Aramaki, Aoba-Ku, Sendai, 980-8579, Miyagi, Japan
e-mail: daisuke.ando.c4@tohoku.ac.jp

K. Yamagishi
e-mail: keisuke.yamagishi.p2@dc.tohoku.ac.jp

Y. Sutou
e-mail: ysutou@material.tohoku.ac.jp

Y. Ogawa
Research Center for Structural Materials, National Institute for Materials Science, 1-2-1 Sengen, Tsukuba, 305-0047, Ibaraki, Japan
e-mail: OGAWA.Yukiko@nims.go.jp

Y. Sutou
Advanced Institute for Materials Research, Tohoku University, 2-1-1 Katahira, Aoba-Ku Sendai, Miyagi, 980-8577, Japan

Keywords

Bcc-magnesium alloy • Shape memory alloy • Aging • Superelasticity

Introduction

Shape memory alloys (SMAs) have attracted attention in several fields owing to their unique properties, such as large recoverable strain and flexibility. The large recoverable strain in SMAs can be obtained upon heating them after unloading (shape memory effect) and/or simply upon unloading (superelasticity) due to reversible martensitic transformation; the strain value generally reaches several percent [1, 2]. Since the discovery of Au–Cd alloy [3], various SMAs have been discovered and developed, e.g., Cu—[4–6], NiTi—[1, 2, 7], Fe—[8–10], and Ti-based alloys [7, 11, 12]; however, Mg-based SMA was not discovered until we first reported the superelasticity of a Mg–Sc alloy [13].

According to reported phase diagrams, the Mg–Sc alloy is the only Mg-based binary alloy whose microstructure can be controlled, depending on heat treatment conditions, between a low-temperature hexagonal close–packed (α) phase and a high-temperature body centered cubic (β) phase at the same Sc content [14, 15]. The unique characteristic of this alloy appears to enable it to show thermoelastic martensitic transformation between β and α″ phases (orthorhombic structure), and we have demonstrated that a Mg-20.5 at.% Sc alloy with β single-phase exhibits superelasticity at 123 K owing to stress-induced martensitic transformation [13]. The working temperature range in which superelasticity occurs depends on the Sc content, and we recently discovered that the Sc content of ∼ 19 at.% is suitable for room temperature superelasticity [16, 17]. Because the density of the superelastic Mg–Sc alloy is ∼ 2 g/cm^3, which is approximately one-third of

S. Barela et al. (eds.), *Magnesium Technology 2023*, The Minerals, Metals & Materials Series,
https://doi.org/10.1007/978-3-031-22645-8_34

conventional NiTi-based superelastic alloys, the alloy may attract attention in automobile and aerospace field from the perspective of fuel efficiency. With its low Young's modulus and high biocompatibility [18, 19], the Mg–Sc superelastic alloy can be applied in medical field as bone plates, stents, etc. Recently, Li et al. implanted a Mg-30 wt.% Sc alloy (equivalent to 18.8 at.% Sc) into rats and showed that the alloy exhibits acceptable biocompatibility and biodegradability [20].

Although the Mg–Sc superelastic alloy exhibits the abovementioned unique properties, it still faces some challenges that need to be addressed. The most critical of which is its low strength and eventual low superelastic recovery at room temperature [16, 17]. Although the recovery can be considerably increased by coarsening the grain size, similar to the case of Cu- and Fe-based shape memory alloy [5, 6, 10], maximum superelastic recovery obtained in Mg−Sc alloy at room temperature was only 3% [16] because slip deformation can occur easily at the same time with stress-induced martensitic transformation. From this perspective, an increase in strength of the β matrix phase is strongly desired to further improve superelasticity.

Herein, we focused on aging heat treatment because age hardening is a well-known strengthening mechanism in various alloys, including Mg-based alloys. The effect of age hardening on superelasticity is also reported in SMAs, such as NiTi—[2, 7], Fe—[8, 9, 21, 22], Ti—[7, 11, 12], and Cu-based alloys [23, 24], where the effect can be either positive or negative depending on the amount and/or size of the aging products. For example, it is reported that nanosized precipitation due to aging heat treatment effectively strengthens the matrix phase of the Fe−Mn−Al−Ni SMA and realizes superior superelasticity, whereas an excess increase in size of the precipitates deteriorates the superelasticity of the alloy [9, 21, 22].

In the Mg−Sc alloy, aging heat treatment is also effective in increasing the hardness and tensile strength owing to the precipitation of the α phase within the β phase [25–27]. However, the Sc content of the measured samples was either 16.8 at.% or > 20 at.% and the effect of aging on superelasticity was not investigated. In this study, we investigated the effect of age hardening on the superelasticity of the Mg −Sc alloy at room temperature.

Procedures

A Mg–Sc ingot with the nominal composition of Mg-18.8 at.% Sc was prepared by OSTECH Co. Ltd. and Hunan Oriental Scandium Co. Ltd. A block was cut from the ingot and hot rolled at 923 K. The resulting sheet was homogenized at 873 K for 24 h before being cold rolled with intermediate annealing at 873 K for 15 min until its thickness reached ∼ 1.3 mm. For each measurement, a specific size of sample was cut from the cold rolled sheet; subsequently, the sample was heat treated and then aged as mentioned below.

The changes in hardness and microstructure were measured using samples with the size of ∼ 5 × 5 mm^2. The samples were solution heat treated at 963 K for 30 min, followed by quenching into iced water to obtain β single-phase, and finally aged at 423, 448, 473, or 523 K for different durations. Hardness was measured using a Vickers hardness tester with an applied load of ∼ 10 N. The hardness of a sample was calculated from the average of 10 points. The microstructure was observed using a scanning electron microscope (SEM) with an accelerated voltage and probe current of 15 kV and 10 μA, respectively. The observed samples were polished using SiC papers and diamond pastes of different grit sizes (3, 1, 0.25 μm) and chemically etched in acid solution for 5 s to obtain a mirror-like surface. X-ray diffraction (XRD) analysis was performed to investigate the constituent phases in measured samples.

Samples with a length and width of approximately 40 and 5 mm were prepared to evaluate superelasticity at room temperature. Cyclic heat treatment (CHT) was applied to the samples to obtain the grain size of ∼ 1 mm because a small grain size of about several hundred micrometers considerably deteriorates superelasticity [16, 17] and therefore makes it difficult to determine the effect of aging on superelasticity. Specifically, the samples were solution heat treated at 963 K for 30 min, followed by air cooling to room temperature. In the following cycle, they were again solution heat treated at 963 K for 30 min, followed by quenching into iced water to obtain β single-phase. This type of abnormal grain growth (AGG) was first observed by Omori et al. in the Cu-based SMA [28], where subgrains seemed to be formed by the precipitation and dissolution of the second phase via CHT, and eventually, the subgrain boundary energy acted as an additional driving force for grain growth, resulting in AGG [28, 29]. The second phase is the α phase in the case of the Mg–Sc alloy [16], and the obtained average grain size was ∼ 980 μm in the current study. The detailed mechanism underlying the AGG is under investigation and will be reported in the future study. The sample that underwent CHT was finally aged at 423 K for 4 ks, and a cyclic tensile test was conducted at room temperature to evaluate the superelasticity of the alloy. The tested sample was loaded to *i*% strain and then unloaded to zero stress at the *i*th cycle (i = 1, 2, 3, etc.). The test was repeated until fracture. The strain rate was set to 10^{-3} s^{-1}, and sample thickness and gauge length were approximately 0.5 and 15 mm, respectively. A sample that underwent CHT without aging heat treatment (as-quenched sample, hereafter) was also tested at room temperature.

Results and Discussion

Figure 1 shows the plots of Vickers hardness versus aging time at different temperatures, where the hardness of the as-quenched sample was ~ 90Hv (shown with a gray shaded line). At each aging temperature, the hardness increases considerably with aging heat treatment and exhibits a sigmoidal change against aging time. Incubation time before the onset of hardening becomes longer with decreasing aging temperature. By contrast, the maximum hardness values of ~ 180 Hv are almost identical within the range of measured aging time.

A microstructural change observed using an SEM is shown in Fig. 2. The as-quenched sample has a β single-phase with a small amount of α phase at the grain boundaries of the β phase (Fig. 2a). These α phases at grain boundaries should be formed during quenching and were also reported in previous studies [13, 15]. Inclusions shown in white in the figure were measured using SEM–EDX (energy dispersive X-ray spectroscopy) and were found to be Sc_2O_3 that could be formed during the melting process. These inclusions are also seen in all the aged samples; therefore, we believe they do not affect the age hardening behavior. Figure 2b presents the microstructure after aging at 423 K for 4 ks, showing the presence of needle-like precipitates within the β matrix phase. These precipitates grow along their longitudinal direction with aging time, and the volume fraction increases, as shown in Fig. 2c and 2d. The same microstructural changes were also seen in the samples aged at 448, 473, and 523 K.

XRD analysis was performed on the samples aged at 423 K to confirm the phase of the precipitates, and the results are shown in Fig. 3. In the XRD pattern, reflection peaks appear at ~ 36.5° after aging for 4 ks, and the peak intensity increases while that of β phase decreases with aging time, indicating that aging products shown in Fig. 2b–d are α phases. Hardness is also plotted in Fig. 4 as a function of the volume fraction of the α phase. The volume fraction was measured using the ImageJ software using the SEM images of the sample aged under different conditions. It is clear from Fig. 4 that the change in hardness due to aging heat treatment is related to the change in the volume fraction of α phase, and an increase in volume fraction of the α phase leads to age hardening in the studied alloy. The same results have been reported in our previous works, where Vickers hardness increases with the volume fraction of needle-like α precipitates due to aging [25–27].

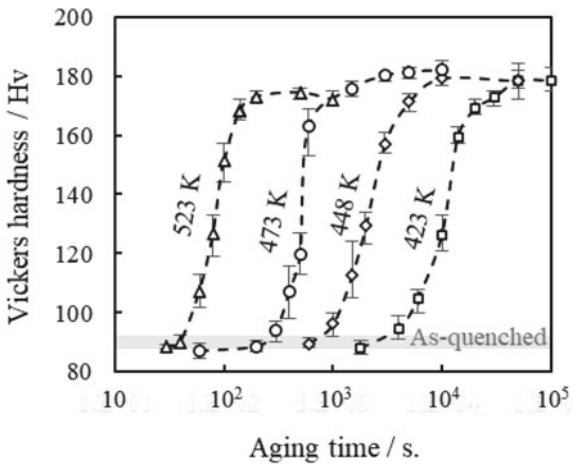

Fig. 1 Vickers hardness as a function of aging time at different temperatures

Arrhenius plots are presented in Fig. 5 to investigate the kinetics of age hardening behavior, where t_c denotes the incubation time, as defined in the inset of the figure, and T represents the aging temperature. According to the Arrhenius equation,

$$\ln\left(\frac{1}{t_c}\right) = -\frac{Q}{\mathrm{RT}} + C,$$

activation energy Q is equivalent to the slope of the Arrhenius plots, where R and C denote the gas constant and a constant value, respectively. The Q value is calculated as ~ 83.9 kJ/mol and is almost the same as the reported one (~ 83.5 kJ/mol) in a previous report which suggests the precipitation of the α phase is dominated by interface diffusion in the present Mg–Sc alloy [27]. Meanwhile, interface diffusion is also dominant in the precipitation of bainite plates in the case of the Cu-based alloy that shows age hardening owing to bainitic precipitation [30]. Furthermore, notably, if the volume fraction is below 30%, the bainite plates can be deformed together with the matrix phase upon stress-induced martensitic transformation and hence do not deteriorate the superelastic recovery at all despite a slight increase in the hardness of the alloy owing to bainite plates [23]. From this perspective, it is expected that α precipitates could also be deformed in the present Mg–Sc alloy upon stress-induced martensitic transformation and, in turn, could improve the superelasticity of the alloy at room temperature if the volume fraction of α precipitates is in a proper range.

To investigate the effect of α precipitates on the superelasticity of the alloy, we conducted cyclic tensile tests at room temperature. The grain size of the tested sample was increased to ~ 980 μm using AGG induced via CHT, as mentioned in Section Procedures. The aging condition was set to 423 K × 4 ks, where the volume fraction of α precipitates was ~ 10%. Notably, the aged samples with higher volume fraction, i.e., the ones aged at 423 K for 10 and 50 ks, were too fragile to undergo cyclic tensile tests. Figure 6a shows the cyclic stress–strain curves obtained using the as-quenched and aged samples. Both samples

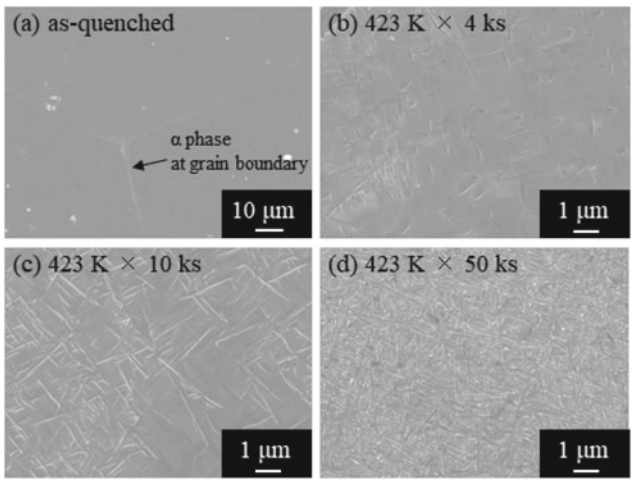

Fig. 2 Secondary electron (SE) images of the samples; **a** as-quenched, **b** after 423 K × 4 ks, **c** after 423 K × 10 ks, and **d** after 423 K × 50 ks

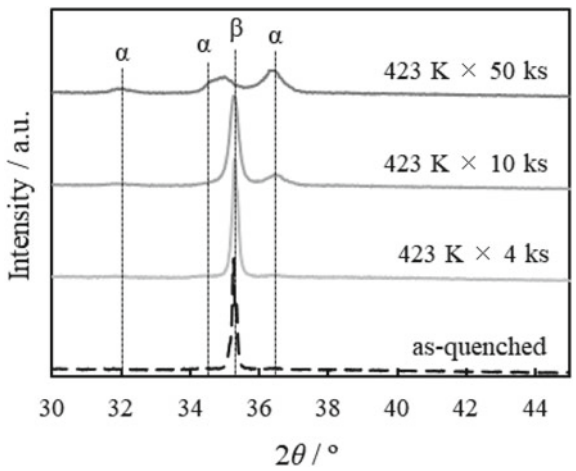

Fig. 3 X-ray diffraction patters obtained from the as-quenched and aged samples

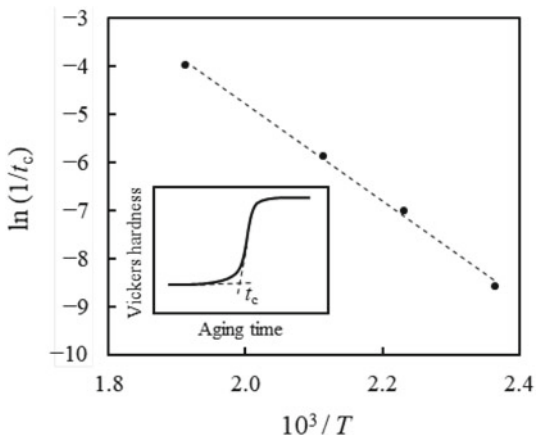

Fig. 5 Arrhenius plots of In ($1/t_c$) versus $1/T.t_c$ denotes the incubation time as defined in the inset of the figure and T represents the aging temperature

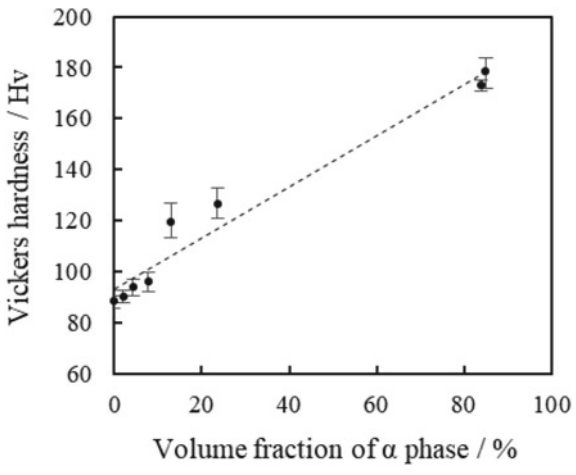

Fig. 4 Vickers hardness as a function of volume fraction of α phase regardless of the aging condition

show clear stress hysteresis during loading and unloading and exhibit superelasticity at room temperature. To compare these two samples quantitatively, superelastic strain (ε^i_{SE}) and applied strain (ε^i_a) at the ith cycle were defined as shown in Fig. 6a. Stress hysteresis (σ^i_{hys}) was also defined as the difference between stresses during loading and unloading at i/2% strain (Fig. 6a). The plots of ε^i_{SE} and σ^i_{hys} as the functions of ε^i_a are presented in Fig. 6b and c, respectively, showing that the maximum superelastic recovery in the aged sample ($\sim$ 1.1%) is higher than that in the as-quenched sample ($\sim$ 0.8%), whereas σ^i_{hys} is slightly decreased in the aged sample. To investigate the possible causes of the differences, SEM observation was performed on the surface of the aged sample after a fracture. Figure 7a and b presents the obtained microstructures, showing that martensite plates have been formed across α precipitates all over the observed

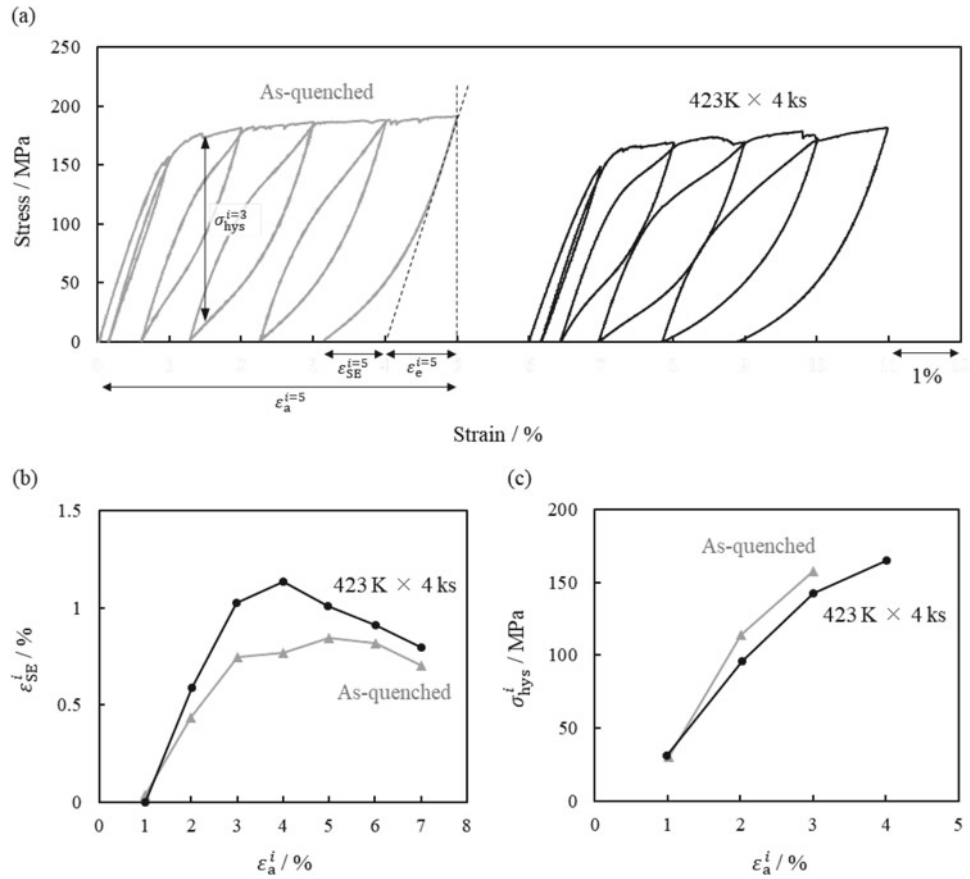

Fig. 6 **a** Comparison of cyclic stress–strain curves at room temperature between as-quenched and aged samples at 423 K for 4 ks. Superelastic strain (ε^i_{SE}), elastic strain (ε^i_e) applied strain (ε^i_a), and stress hysteresis (σ^i_{hys}) at *i*th cycle are also defined in the figure. **b** ε^i_{SE}, and **c** σ^i_{hys} of the samples as the function of ε^i_a

area and the precipitates seem to be deformed along with the β matrix phase upon stress-induced martensitic transformation, as in the case of the foregoing Cu-based superelastic alloy [23, 30]. It is therefore suggested that α precipitates that had been deformed along with β matrix phase cause back stress to assist the reverse transformation of the stress-induced martensite phases. The back stress and a slight increase in hardness might result in decreased stress hysteresis and slightly larger superelastic recovery.

Conclusions

The effect of aging heat treatment on the hardness, microstructure, and superelasticity of the Mg-18.8 at.% Sc alloy at room temperature was investigated herein, and the following conclusions were drawn:

(1) Aging heat treatment at temperatures between 423 and 523 K effectively increased the Vickers hardness of the alloy from ∼ 90 Hv (as-quenched condition) to the maximum value of 180 Hv.

(2) SEM observations and XRD analysis revealed that the precipitation of the α phases within the β matrix phase caused age hardening and the hardness value after aging almost linearly depended on the volume fraction of the α phase regardless of the aging condition.

(3) The cyclic tensile test of the sample that had been aged at 423 K for 4 ks revealed that it was possible for the α precipitates with a volume fraction of ∼ 10% to be deformed along with the β matrix phase of the alloy upon stress-induced martensitic transformation, which in turn caused back stress during reverse transformation. The back stress and a slight increase in hardness of the aged sample might result in slightly smaller stress hysteresis and minor improvement in superelastic recovery at room temperature compared with those of the as-quenched sample.

Acknowledgements This work was supported by JSPS KAKENHI [grant numbers 21J12146, 18H01691] and the Adaptable and Seamless Technology Transfer Program through target-driven R&D (A-STEP) from Japan Science and Technology Agency (JST) [grant number JPMJTR20TJ].

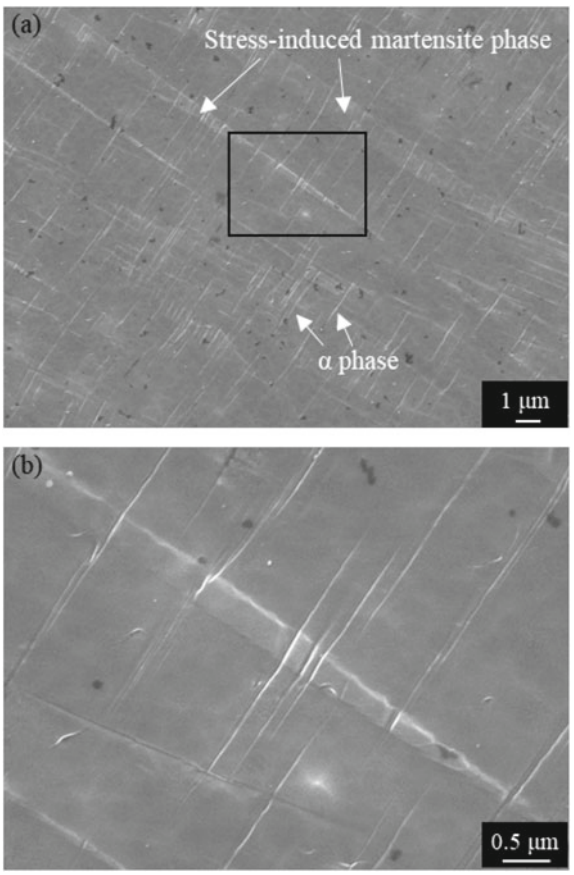

Fig. 7 Secondary electron (SE) images of the aged samples at 423 K for 4 ks after fracture: **a** low and **b** high magnification images

References

1. Otsuka K, Shimizu K (1986) Pseudoelasticity and shape memory effects in alloys. Int. Met. Rev. 31:93–114.
2. Miyazaki S, Otsuka K (1989) Development of shape memory alloys. ISIJ Int. 29:353–377.
3. Ölander A (1932) An electrochemical investigation of solid cadmium-gold alloys. J. Am. Chem. Soc. 54:3819–3833.
4. Otsuka K, Wayman CW, Nakai K, Sakamoto H, Shimizu K (1976) Superelasticity effects and stress-induced martensitic transformations in Cu-Al-Ni alloys. Acta Metall. 24:207–226.
5. Sutou Y, Omori T, Yamauchi K, Ono N, Kainuma R, Ishida K (2005) Effect of grain size and texture on pseudoelasticity in Cu-Al-Mn-based shape memory wire. Acta Mater. 53:4121–4133.
6. Sutou Y, Omori T, Kainuma R, Ishida K (2013) Grain size dependence of pseudoelasticity in polycrystalline Cu-Al-Mn-based shape memory sheets. Acta. Mater. 61:3842–3850.
7. Miyazaki S (2017) My experience with Ti-Ni-based and Ti-based shape memory alloys. Shap. Mem. Superelasticity 3:279–314.
8. Tanaka Y, Himuro Y, Kainuma R, Sutou Y, Omori T, Ishida K (2010) Ferrous polycrystalline shape-memory alloy showing huge superelasticity. Science 327:1488–1490.
9. Omori T, Ando K, Okano M, Xu X, Tanaka Y, Ohnuma I, Kainuma R, Ishida K (2011) Superelastic effect in polycrystalline ferrous alloys. Science 333:68–71.
10. Omori T, Okano M, Kainuma R (2013) Effect of grain size on superelasticity in Fe-Mn-Al-Ni shape memory alloy wire. APL Mater. 1:032103.
11. Miyazaki S, Kim HY, Hosoda H (2006) Development and characterization of Ni-free Ti-base shape memory and superelastic alloys. Mater. Sci. Eng. A 438–440:18–24.
12. Kim HY, Miyazaki S (2015) Martensitic transformation and superelastic properties of Ti-Nb base alloy. Mater. Trans. 56:625–634.
13. Ogawa Y, Ando D, Sutou Y, Koike J (2016) A lightweight shape-memory magnesium alloy. Science 353:368–370.
14. Beaudry BJ, Daane AH (1969) A study of the scandium-magnesium system from 0 to 60 at.% scandium. J. Less-Common Met. 18:305–308.
15. Ogawa Y, Ando D, Sutou Y, Yoshimi K, Koike J (2016) Deformation of α/β phase boundaries and mechanical characterization of Mg-Sc binary alloys. Mater. Sci. Eng. A 670:335–341.
16. Yamagishi K, Ogawa Y, Ando D, Sutou Y, Koike J (2019) Room temperature superelasticity in a lightweight shape memory Mg alloy. Scr. Mater. 168:114–118.
17. Yamagishi K, Ando D, Sutou Y, Ogawa Y (2020) Texture formation through thermomechanical treatment and its effect on superelasticity in Mg-Sc shape memory alloy. Mater. Trans. 61:2270–2275.
18. Zheng YF, Gu XN, Witte F (2014) Biodegradable metals. Mater. Sci. Eng. R 77:1–34.
19. Haghshenas M (2017) Mechanical characteristics of biodegradable magnesium matrix composites: A review. J. Magnes. Alloys 5:189–201.
20. Liu J, Lin Y, Bian D, Wang M, Lin Z, Chu X, Li W, Liu Y, Shen Z, Liu Y, Tong Y, Xu Z, Zhang Y, Zheng Y (2019) *In vitro* and *in vivo* studies of Mg-30Sc alloys with different phase structure for potential usage within bone. Acta. Biomater. 98:50–66.
21. Ozcan H, Ma J, Wang SJ, Karaman I, Chumlyakov Y, Brown J, Noebe RD (2017) Effects of cyclic heat treatment and aging on superelasticity in oligocrystalline Fe-Mn-Al-Ni shape memory alloy wires. Scr. Mater. 134:66–70.
22. Tseng LW, Ma J, Hornbuckle BC, Karaman I, Thompson GB, Luo ZP, Chumlyakov YI (2015) The effect of precipitates on the superelastic response of [100] oriented FeMnAlNi single crystals under compression. Acta Mater. 97:234–244.
23. Sutou Y, Koeda N, Omori T, Kainuma R, Ishida K (2009) Effects of aging on stress-induced martensitic transformation in ductile Cu-Al-Mn-based shape memory alloys. Acta Mater. 57:5759–5770.
24. Kainuma R, Yoshinaka Y, Omori T (2018) Cyclic properties of superelasticity in Cu-Al-Mn single-crystalline sheets with bainite precipitates. Shap. Mem. Superelasticity 4:428–434.
25. Ando D, Ogawa Y, Suzuki T, Sutou Y, Koike J (2015) Age-hardening effect by phase transformation of high Sc containing Mg alloy. Mater. Lett. 161:5–8.
26. Ogawa Y, Ando D, Sutou Y, Koike J (2016) Aging effect of Mg-Sc alloy with α+β two-phase microstructure. Mater. Trans. 57:1119–1123.
27. Ogawa Y, Sutou Y, Ando D, Koike J (2018) Aging precipitation kinetics of Mg-Sc alloy with bcc+hcp two-phase. J. Alloys Compd. 747:854–860.

28. Omori T, Kusama T, Kawata S, Ohnuma I, Sutou Y, Araki Y, Ishida K, Kainuma R (2013) Abnormal grain growth induced by cyclic heat treatment. Science 341:1500–1502.
29. Kusama T, Omori T, Saito T, Kise T, Tanaka T, Araki Y, Kainuma R (2017) Ultra-large single crystals by abnormal grain growth. Nat. Commun. 8:354.
30. Sutou Y, Koeda N, Omori T, Kainuma R, Ishida K (2009) Effects of ageing on bainitic and thermally induced martensitic transformations in ductile Cu-Al-Mn-based shape memory alloys. Acta Mater. 57:5748–5758.